Optical Engineering

SPIEDigitalLibrary.org/oe

Large-field high-resolution mosaic movies

Robert H. Hammerschlag
Guus Sliepen
Felix C. M. Bettonvil
Aswin P. L. Jägers
Peter Sütterlin
Yong Lin
Sara F. Martin
Olga Panasenco
Eugene P. Romashets

SPIE

Large-field high-resolution mosaic movies

Robert H. Hammerschlag
Leiden Observatory
P.O. Box 9513
2300 RA Leiden, the Netherlands
and
Utrecht University
Department of Physics & Astronomy
Postbus 80000
3508TA Utrecht, the Netherlands
E-mail: R.H.Hammerschlag@astro-uu.nl

Guus Sliepen
Royal Swedish Academy of Sciences
Institute for Solar Physics
AlbaNova University Center
10691 Stockholm, Sweden

Felix C. M. Bettonvil
Leiden Observatory
P.O. Box 9513
2300 RA Leiden, the Netherlands
and
NOVA Op-IR group at ASTRON
P.O.Box 2
7990AA Dwingeloo, the Netherlands

Aswin P. L. Jägers
Utrecht University
Department of Physics & Astronomy
Postbus 80000
3508TA Utrecht, the Netherlands

Peter Sütterlin
Royal Swedish Academy of Sciences
Institute for Solar Physics
AlbaNova University Center
10691 Stockholm, Sweden

Yong Lin
University of Oslo
Institute for Theoretical Astrophysics
P.O. Box 1029
Blindern, N-0315 Oslo 3, Norway

Sara F. Martin
Olga Panasenco
Eugene P. Romashets
Helio Research
5212 Maryland Avenue
La Crescenta, California 91214

Abstract. Movies with fields-of-view larger than normal, for high-resolution telescopes, will give a better understanding of processes on the Sun such as filament and active region developments and their possible interactions. New active regions can serve as an igniter of the eruption of a nearby filament. A method to create a large field-of-view is to join several fields-of-view into a mosaic. Fields are imaged quickly, one after another, using fast telescope-pointing. Such a pointing cycle has been automated at the Dutch open telescope (DOT), a high-resolution solar telescope located on the Canary Island La Palma. The number and positions of the subfields are calculated automatically and represented by an array of bright points in the guider image which indicates the subfield centers inside the drawn rectangle of the total field on the computer screen with the whole-sun image. Automatic production of flats is also programmed. For the first time, mosaic movies were programmed from stored information on automated telescope motions. The mosaic movies show larger regions of the solar disk in high resolution and fill a gap between available whole-sun images with limited spatial resolution of synoptic telescopes including space instruments and small-field high-cadence movies of high-resolution solar telescopes. [DOI: 10.1117/1.OE.52.8.081603]

Subject terms: mosaic movies; solar observations; high-resolution movies; large-field movies; automatic calculation of subfields; whole-sun images.

Paper 121301SSP received Sep. 13, 2012; revised manuscript received Nov. 19, 2012; accepted for publication Dec. 5, 2012; published online Jan. 31, 2013.

1 Introduction

Small-sized solar telescopes, that make images of the whole solar disk in low spatial resolution, are the so-called synoptic solar telescopes. Relatively slow, long-term changes, on large spatial scales, are typically observed along with occasional short-term solar eruptive events such as flares, erupting filaments, and coronal mass ejections (CME's). These small-sized telescopes are operating both on the ground and in space, the latter ones, specifically, to study the very hot, but very tenuous and irregular extensive outer solar atmosphere, the corona, in ultraviolet and x-ray radiation. On the other hand, high-resolution solar telescopes observe only a small part of the whole solar disk, particularly in dedicated program campaigns of typically 10 to 15 days.

Between these two modes of solar observations, is a current-day gap of high-resolution observations of larger areas on the Sun. An attractive method of filling this gap is the production of mosaic movies with high-resolution telescopes, as discussed herein. In our application, a "mosaic" is a set of adjacent, slightly overlapping images covering a larger area of the Sun than the field-of-view designed for a given telescope. Mosaic movies reveal the dynamic developments of solar features, in high resolution, over large areas on long timescales. The technique of making mosaic movies is needed for understanding the building-up and storage of energy, in the solar atmosphere, that can lead to eruptive events like flares and CME's. Prominences and filaments play an important role in these processes. Prominences are complex systems of large, continuously changing threads of ionized gas that are two orders of magnitude denser than the surrounding coronal atmosphere. Prominences are called filaments when seen in front of the solar disk. The filaments scatter light from the solar disk and are visible as dark structures against the solar disk, whereas, they are bright when seen above the limb. An overview on this subject is given in Ref. 1. Understanding these dynamic structures, and making numerical calculations, require observations of higher spatial resolution than usually obtained with synoptic telescopes.

The production of mosaics from time sequences of images in general is known. Especially, production of panoramas from video sequences is extensively studied.[2] Also, the registration of dynamic effects in panoramas has been studied.[3] However, the production of those mosaics starts from completely different image sequences than in high-resolution solar observations. The mosaics in the literature are formed from (hand) moving video cameras without registration of place of the individual images. However, the successive images have a large overlap, mostly 50 percent or more. Pairs of successive images are compared and combined. On the contrary, the images of solar observations have minimum overlap in space in order to cover a certain field with a minimal number of exposures. It reduces the time needed for one mosaic and, consequently, improves the time cadence of the mosaics. A first ordering of the images and identification of mosaic cycles is done, a posteriori, using the telescope pointing and time which are recorded together with the images. A special algorithm has been developed for this ordering. In case an observer changes the mosaic field while observing, for instance to follow certain events on the sun, the algorithm will find, afterwards, the mosaics both from before and after changing the field and even partial mosaics which were not completed. Correct alignment and merging of images required the development of new combinations of techniques because of the presence of image distortions by the earth's atmosphere. In comparison with normal imaging, like for panorama mosaics, high-resolution telescope imaging is much more sensitive to these atmospheric disturbances, usually called seeing. Specifically, minimization of the root-mean-square differences between neighboring images in the overlapping field parts, simultaneously both in space and time, is new. Hence, no separate mosaics in space are formed, but the optimum positioning of the individual images takes place three-dimensionally in space and time together.

Sections 2 and 3 describe the newly developed methods. Afterwards, the practical use of the system is discussed in Sec. 4. The very diverse possibilities are illustrated with a few examples. The last one shows special possibilities by combining two co-observing high-resolution telescopes.

2 Mosaic Movies

The guider software, at the Dutch open telescope (DOT),[4–6] maintains a log of the pointing of the telescope and the information from this log is used to, a-posteriori, identify mosaic cycles. Consecutive runs of identical cycles form a mosaic movie. The images, that belong to a mosaic cycle, are then identified and the pointing information from the guider log is used to prealign the images and to constrain the solution space in case the actual alignment algorithms can give multiple solutions.

In assembling sets of adjacent individual images of the Sun into mosaic cycles and then into mosaic movies, there are several problems to overcome. The first is to identify which images belong where in each mosaic cycle. Although it is possible to start an explicit mosaic observation sequence, where the number of images in space and time are known beforehand, and store this information in the flexible image transport system (FITS) image headers, we have chosen to keep our telescope-control software mostly unaware of mosaic cycles, therefore, this information is not readily available. Consequently, we must reconstruct, afterwards, if and how many distinct mosaic cycles were recorded and where each image is to be placed in each mosaic cycle. Although this is labor-intensive, it has the advantage of being more flexible. For example, though the DOT guider software has an option to generate a pointing pattern for automatically producing of a mosaic cycle and a mosaic movie, it is not necessary to use this functionality. It is also possible to allow an observer to use his own tools to generate pointing patterns, or to even specify them manually, without having to worry about creating correct FITS headers for further processing. Any changes necessary for the mosaic reconstruction software can be done afterwards.

The second problem is to correctly align the images that make a mosaic movie both in time and space. Experience has shown, that first assembling individual mosaics, and afterwards making a movie of those mosaics, is not ideal. Since observing through the atmosphere causes time-varying distortions of the image of the Sun, while the Sun itself is changing continuously, there will be small errors when combining several images into a mosaic. Typically, one tries to minimize the root-mean-square difference between the images in the regions where they overlap. However, when making a movie of these individual mosaics, there will be errors between successive mosaics which are pronounced for two reasons. The first is the overlap between adjacent images in a mosaic is usually between 5 percent and 25 percent, whereas, the overlap between successive images at the same solar position in a mosaic is close to 100 percent. Therefore, the error integrated over the whole field-of-view is much larger. Second the human vision system is very good at detecting motion in time. The best approach, therefore, is to optimize all the images that make up the mosaic movie together, trying to minimize the root-mean-square difference both in space and time.

Since it is always best to have a fast cadence when making movies, the overlap between images in a mosaic should be as small as possible because this reduces the number of images necessary to cover a certain area. Due to the use of an equatorial mount at the DOT, the "up" direction in the recorded images always corresponds to the direction of the earth north pole and there is no diurnal rotation of the solar image. When using an alt-azimuth mount, one has to account for image rotation when making mosaic movies. The presented algorithm is able to handle this image rotation. This has been demonstrated on the Swedish Solar Telescope (SST).[7] However, larger numbers of image fields are necessary to cover a specified mosaic field due to the image rotation.

To ensure individual images can be aligned to each other, it is best to point the telescope in a boustrophedonic pattern (making alternate linear scans in opposite directions), such that, there is always overlap at one of the edges between two consecutive images, except for when the telescope has reached the last point of a cycle and moves back to the first (see Fig. 1).

3 Method

An algorithm is presented that, fully automatically, creates mosaic movies from a given set of images and a guider log without having to manually specify any information about the mosaics.

The algorithm for determining mosaic cycles is as follows:

1. The list of images is sorted by time.
2. For each image, the pointing coordinates at the time of the exposure are retrieved.
3. Similar coordinates are given a unique number. The first coordinate-pair is given the coordinate-number one. The next coordinate-pair is compared with the previous coordinate-pairs. If the distance is less than a predefined maximum deviation $d_{\max}$, the next coordinate-pair is given the same coordinate-number as the one it is close to. If it is not close to any previous coordinate-pair, it is given the next available coordinate-number.
4. A histogram is made of each possible combination of two coordinate-numbers against how often these two coordinate-numbers are exposed directly after each other.
5. Using this histogram, for each coordinate-number i, the most likely successor coordinate-number $N(i)$ is determined. If the contribution of this successor coordinate-number is less than 50 percent, it is discarded.
6. Consecutive coordinate-numbers form a cycle if, when starting at i and following the most likely successors $N(i)$, $N(N(i))$, et cetera, one ends back at i. Distinct cycles are given a number as well. The first coordinate-number belongs to the first cycle numbered one. Then, every following successor coordinate-number $N(i)$, $N(N(i))$, ... also belongs to cycle number one. The next coordinate-number that does not belong to the first cycle then belongs to cycle number two, and so on.

After a mosaic cycle has been found, the images are aligned using the following algorithm:

1. Images are prealigned using the coordinates from the guider log.
2. The optimal alignment between pairs of overlapping images (both in time and space) is calculated using a cross-correlation algorithm.
3. For each overlapping pair, a virtual spring is created between the two images which has a rest length that corresponds to the optimal alignment of the pair and a configurable spring constant (see Fig. 2).

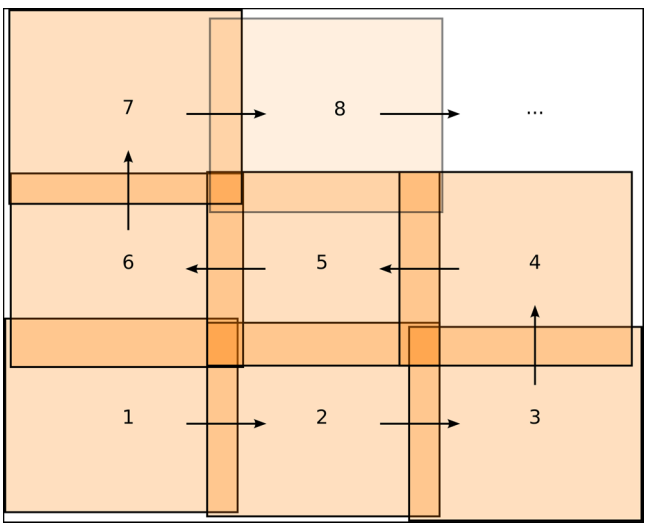

Fig. 1 A boustrophedonic pattern, making alternate linear scans in opposite directions, is a good way to create a mosaic. At the bottom row, the telescope moves to the right after each image. At the end of the row, the telescope moves one image up, then continues to the left, and so on. In this way, there is always overlap between consecutive images in one mosaic.

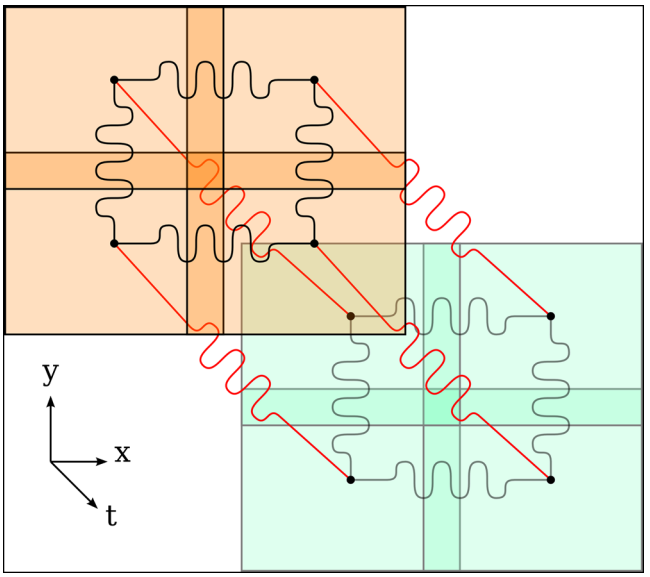

Fig. 2 Springs between images in a mosaic movie. The upper-left orange area is the first mosaic of a 2×2 image mosaic movie. Horizontal and vertical black springs connect images neighboring in space. The lower-right green area is the second mosaic. The diagonal red springs connect images neighboring in time.

4. In a loop, the forces exerted by the springs on all the images are calculated and the images are moved a fraction in the direction proportional to the force. This is repeated until the amount of movement drops below a certain level or until this step has been repeated a fixed number of times.
5. A bounding box is calculated for the entire mosaic movie and all the images are shifted such that the top left corner of the bounding box is at coordinates (0,0).
6. For each mosaic, an initially completely transparent frame is created with the same size as the bounding box around the whole mosaic. Each image is placed at the calculated position in that frame.
7. Within each mosaic of the mosaic movie, the images created in the previous step are blended together using Enblend.[8]
8. From the individual mosaics, a movie is created using a movie creation tool such as Mencoder.[9]

Due to seeing, each image will be distorted slightly different and, even after a perfect alignment of whole images, distortions inside individual images in a mosaic movie will result in visible image motion in the movie. This can be reduced by splitting images in sets of smaller, overlapping patches. These patches can all be coupled to their neighbors in time, thereby, reducing visible image motion of these patches.

3.1 *Guider-Assisted Cross-Correlation*

The optimal alignment, between two neighboring images, can be determined using a cross-correlation algorithm. The fastest way is using fast Fourier transforms (FFT) to reduce the cross-correlation to a simple multiplication in Fourier space. This, also, efficiently allows a convolution filter to be applied.[10] A high-pass filter is recommended to remove any intensity gradients caused by the telescope optics. After transforming the result back, the position of the intensity peak, in the resulting correlation image, corresponds to the most likely shift between the two images. This position can be estimated, with subpixel accuracy, by fitting a 2D Gaussian curve to a 3×3 pixel region around the intensity peak.[11] The problem with the FFT based method is that the peak is not uniquely defined, instead, it is the position of the true peak modulo, the image width, and height. For example, for a 1024×1024 pixel image, if the position of the intensity peak is at coordinates (40, 1000) then, assuming that the two images do really overlap, the true peak could be at (−984, 1000), or at (40, −24), or at (−984, −24). The ambiguity can be removed by choosing the coordinate that is closest to the coordinates from the guider log.

3.2 *Spring Relaxation*

There are several types of springs that represent the relation between individual images:

- Springs with very weak spring constants that couple images to their prealignment positions according to the guider log. This prevents the whole mosaic from drifting since only the guider log contains absolute positions.
- Springs with normal spring constants that couple images to their direct neighbors in space, however, the strength should also be inversely proportional to the time between the exposures of those images.
- Springs with strong spring constants that couple images to their direct neighbors in time.
- Optionally, if there is a specific region of interest in which image motion should be minimized, the spring constants between images neighboring in time in that region should have an even stronger spring constant. Consequently, the surrounding images will then move more strongly.

For an $N_x \times N_y \times N_t$ image mosaic movie, where N_x is the number of images in the horizontal direction, N_y in the vertical direction, and N_t the number of mosaics in the mosaic movie, there will be approximately $3\ N_x \times N_y \times N_t$ springs.

For each image i, we keep track of the estimated position $\vec{r}_i$, that initially is set to be equal to the position according to the guider log. For each of these springs, the spring force between images i and j is $\vec{F}_{ij} = k_{ij}(\vec{r}_{ij} - \vec{R}_{ij})$, where $\vec{r}_{ij} = \vec{r}_i - \vec{r}_j$ is the estimated distance vector between the two images, $\vec{R}_{ij}$ is the optimal distance between the two images according to the cross-correlation algorithm, and k_{ij} is the spring constant for this pair. After calculating all the forces, we calculate an improved estimate of the position of the images: $\vec{r}_i' = \vec{r}_i + c\sum_j \vec{F}_{ij}$, where $c << 1$ is a small constant that limits the amount of movement in a single relaxation step and ensures the algorithm will converge smoothly to a solution. We repeat this a fixed number of steps or until the total force on each image, $\sum_j \vec{F}_{ij}$, is lower than a certain threshold.

3.3 *Seamless Blending*

After calculating the optimal positions of all the images in the mosaic movie, the images, within each mosaic of the movie, must be blended together. Simply overlaying the images on top of each other will result in sharp, visible seams between the individual images. This can be avoided by making the images partly transparent in the overlapping region, such that, they are blended gradually into each other. While that avoids a sharp seam, it can still result in image artifacts when the images are not perfectly aligned. A much better way is to use "seam-line optimization", an algorithm where an optimal curve is determined in the overlapping region that minimizes visual artifacts. Along the curve, the width of the blending region is varied depending on the intensity gradient of the image across the curve. In areas with small gradients (and thus low contrast), a wide region is used to blend, whereas, areas with large gradients (high contrast) use short region to blend. The off-the-shelf, open source program "Enblend"[8] implements this algorithm. As input, this program expects a set of images the size of the whole mosaic, each input image containing the original image already aligned, and with an alpha layer that is opaque where the original image is, and transparent everywhere else.

4 Practical Use and Results

4.1 *Description of the System*

The observer uses the whole-sun image of the telescope guider to choose the place of interest and its size by drawing

a rectangle around the desired region. Subsequently, the program calculates the required number of telescope fields-of-view and the coordinates of each field to be successively observed.

Figure 3 shows an example on an image from the guider telescope of the DOT. The guider telescope is equipped with an $H\alpha$ filter and electronic enhancement of contrast, of the image, for good visibility of filaments and prominences. Bright-yellow lines indicate the chosen rectangle. In this example, the calculated number of fields is 12 in the east-west direction six, and in the south-north direction two (north is on top, east at the left, like in the hand-control panel on the left side of the image). The calculated centers of the fields are indicated by bright-yellow points.

During its exposure, the first mosaic field is shown in the bottom-left corner of the total mosaic field in Fig. 3(a). The boundaries of this field are indicated by a dark-red rectangle corresponding with the smallest camera field currently in use of 91×72 arcsec, being 1300×1030 pixels, hence, pixel size 0.07×0.07 arcsec. The small dark-purple circle indicates the target position for tracking.

The DOT is equipped with a multi-channel system. The channels, at the blue side of the spectrum, are equipped with KPF100 Hitashi Denshi cameras. At present, the wavelengths of these channels are (i) G-band 430.5 nm, width 1.0 nm, (ii) blue continuum 431.9, width 0.6 nm, (iii) Ca II-H 396.87 nm, width 0.13 nm tunable to blue by tilt, (iv) Ba II 455.4 nm, width 0.008 nm tunable $-/+0.2$ nm birefringent Irkutsk filter[12,13] and (v) near Barium blue continuum 450.48 nm, width 0.54 nm or H-beta prominence 486.23 nm, width 0.15 nm tunable to blue by tilt. The channels, at the red side of the spectrum, are equipped with ES4020 MegaPlusII Redlake cameras with a field of 113×113 arcsec, 2048×2048 pixels binned 2×2 to effective 1024×1024 pixels of 0.11×0.11 arcsec. These channels are (i) $H\alpha$ 656.28 nm, width 0.025 nm tunable $-/+0.8$ nm birefringent Zeiss filter[14] and (ii) red continuum 655.05 nm, width 0.24 nm or $H\alpha$ prominence 656.35 nm, width 0.23 nm tunable to blue by tilt.

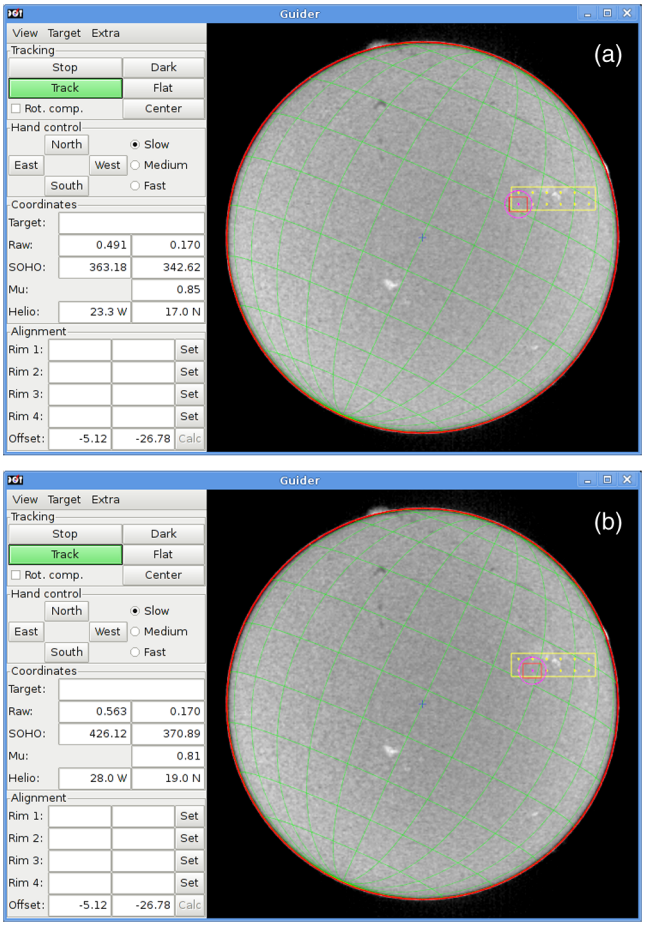

Fig. 3 Guider-telescope images of the whole sun with a mosaic field of six by two fields. Image (a) taken during the observation of the first sub-field of the mosaic. Image (b) taken during the second subfield observation. The array of bright points indicates the subfield centers.

The image *b*, in Fig. 3(b), shows the guider image during the exposure of the second mosaic field. The dark-red boundary of the rectangular field is shifted one position to the right, to the west. The observer can follow how the field is moving along the programmed path starting at the bottom-left corner, then moving one-by-one to the right, in this case, six positions then one position upward, followed by moving back one by one to the left. In this example, there only are two rows. In case of more rows, the field continues by going up one position at the left side followed by going step by step to the right and so on, as already explained in Fig. 1. When the last field is reached, the telescope automatically moves to the first field at the bottom-left corner.

Originally, the program was developed with a square region of interest in mind, such as 2×2, 3×3 or 4×4 fields. In the case of an elongated region, it would be better to go step by step along the shortest side of the region instead of along the longest side. This will give the best fit of the field boundaries to each other because the maximum time difference, between neighboring fields, is minimized. The program will be improved in this way for future observations.

The DOT has an equatorial mount. Consequently, the boundaries of the camera fields do not rotate relative to the solar image. This is comfortable, especially during long-term mosaic movies over several hours. Alt-azimuth mounts show relatively fast image rotation in the neighborhood of the zenith position. Hence, such rotation will be maximal during the hours around noon in summer. Of course, this could be overcome by an image rotator which requires additional optical surfaces and a precision drive system. The camera-field boundaries at the DOT are oriented east-west and north-south. This is convenient both for east-west strips (as in our example) and for north-south strips. In practice, these strips can be valuable for filament observations with the $H\alpha$ filter tuned to several spectral-line wing positions (a certain distance to the $H\alpha$ line center corresponds to a certain line-of-sight velocity). Flows, parallel to the solar surface, have a line-of-sight and transverse component except under specific limited circumstances when the flows are entirely in the plane of the sky. The selection of a line-of-sight velocity value can be helpful to find gas streams with certain velocities along the solar surface.

The large dark-red circle along the rim (see Fig. 3) indicates that the main telescope is precisely following the Sun, by use of an active system, which processes the solar rim position information of the guider. The guider image can be observed in full screen, see Fig. 4, to allow a better observation of objects of possible interest on the solar disk and at

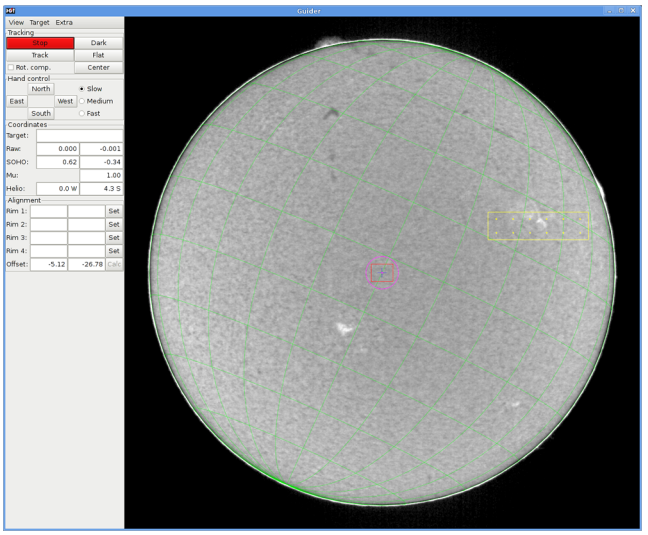

Fig. 4 Full-screen guider image for a better visibility of objects of interest. The dark red ring at the rim is absent because active guiding is switched off. Details outside the rim, like prominences, are better visible by use of electronic enhancement. The main telescope is pointed to the disk center.

the rim. Before the start of the mosaic observations, the main telescope can follow the sun passively by use of only coordinates. The broad red ring disappears and what remains is a thin bright ring which is due to electronic enhancement of the region outside the rim for a better visibility of the prominences. Exactly at the rim, a narrow green ring of the solar coordinate system is visible. The position of the main telescope is visible in Fig. 4 at the disk center indicated by the purple circle and red camera-field boundary.

4.2 *Application Examples*

The mosaic-movie technique is extremely useful in correctly identifying and analyzing the dynamics of solar features as we illustrate by referring to common solar features seen in Fig. 5. This mosaic consists of 12 fields from a mosaic movie in the $H\alpha$ line center, as described above. It was recorded during the 2010 DOT Prominence Project by a team of collaborating solar researchers (PROM) coordinated by Helio Research[15] in La Crescenta, California. Successive mosaics, of this area, were recorded during 10 days for the purpose of observing filament channels and filaments forming around the periphery of two relatively new, small active regions. One new filament channel is designated by three arrows and a label in Fig. 5 at the left (eastern) side of the mosaic. This filament channel contains a small filament in its initial stage of formation. Several other filaments are shown by arrows and labels. All are in filament channels, or zones, where the magnetic field of the central part of the channel is parallel with the long axis of the filament. The pattern of fibrils, typical of a filament channel, can be seen in the filament channel in the left side of the mosaic image in Fig. 5. The fibrils align end-to-end along boundaries where the line-of-sight component of the magnetic field direction changes sign from outward to inward. This is seen when Fig. 5(a) is compared to Fig. 5(b). Similar major channels, of realigned fibrils, are

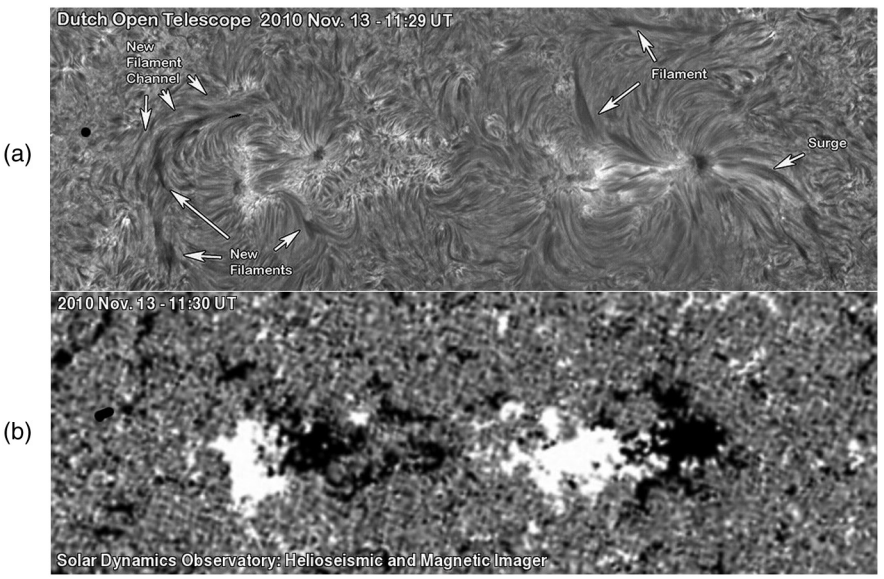

Fig. 5 (a) Mosaic of 6 × 2 images in the $H\alpha$ line center from a mosaic movie over 5.5 h on this same area. This image was taken at 11:29 UT (10:19 local solar time) 0.2 h after the start of the mosaic sequences of images. Movies are an important asset to correct identifications of all of these dynamic solar features which change at different rates. The main subjects are two "active regions," one left of center, and the other right of center. Each active region consists of bright areas called "plage." Within these brightened areas, are sunspots which are the compact, nearly round, dark areas. Everywhere around the plage and sunspots are elongated, thread-like structures known as "fibrils" which are organized in patterns around the plage and sunspots because they follow the direction of the local magnetic field. The organized fibril patterns enable the identification of the boundaries of the active regions which are often also marked by dark "filaments." Mosaic movies were taken of these two regions to study the formation and evolution of filaments that develop in and around the active regions. The filaments are designated by arrows with the exception of the arrow furthest to the right side of the image which points to a short-lived feature called a "surge." In a single image, a narrow "surge" of mass along the local magnetic field can appear similar to a filament, but a surge is a temporary ejection of mass lasting minutes whereas filaments are longer-lived dynamic structures that develop specifically at boundaries where the local magnetic field has a sharp reversal from positive to negative polarity. (b) Magnetogram of same region at same time with SDO (Solar Dynamics Observatory) in space. Noticeably the DOT mosaic has a higher resolution: pixel size 0.1 arcsec at DOT, 0.5 arcsec at SDO.

expected to form between the two active regions over the course of several days and later between the sunspots within each active region.

An example of a surge is shown by the arrow that is furthest to the right in Fig. 5. Surges are short-lived ejections that emanate from specific locations that are often close to flare footpoints in the $H\alpha$ chromosphere. Their curved trajectories indicate that their flows follow the local magnetic field and reveal the degree of local field curvature. The example, in Fig. 5, has little obvious curvature as it follows the nearly radial fibrils around the periphery of the closest sunspot. As in this case, in a single image, a surge can roughly resemble a filament, however, in the movie, this surge is readily distinguished from filaments because its flows are more rapid and shorter-lived than the typical flows in filaments. It is seen, that the surge is no longer present in the series of three images, shown in Fig. 6, at a later time during the same day.

The time between successive images is 6 min and 36 s, as shown in Fig. 6. The contrast of the structure, in the field around the flare, is seemingly lower in the bottom mosaic than in the two previous ones. This is because the program, to represent the mosaic on the screen, has an automatic contrast adaption to be able to clearly show the full range of intensities in the image, especially during a solar flare.

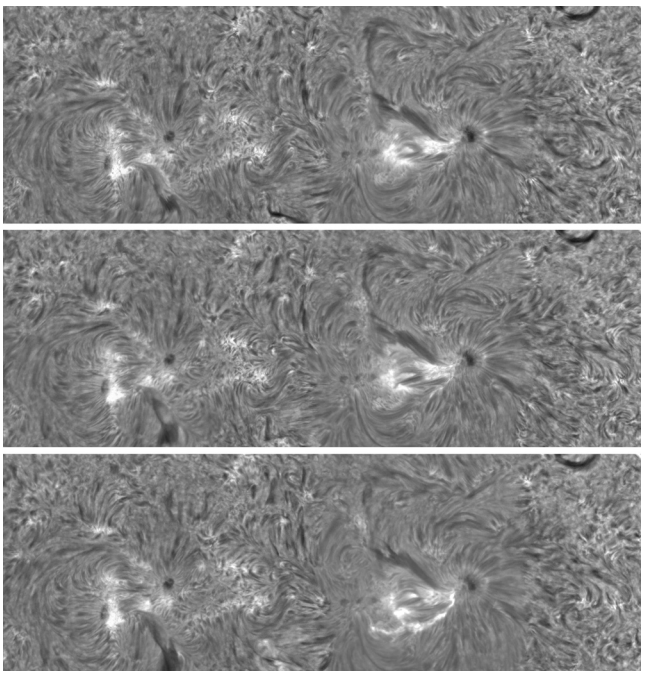

Fig. 6 Three successive images from the same set of 12 fields-of-view as in Fig. 5 at 4.7 h after the start of the observations on this day. The fibrils between the sunspots are one of the special subjects of interest. If they are dark and are changing rapidly, as within the plage to the left of the large sunspot in the active region in the right side of these images, they will have larger Doppler shifts than other fibrils. These large Doppler shifts are a characteristic property of locations where new magnetic flux is welling up beneath the fibrils. The dark fibrils are called "arch filament systems." All active regions begin as "emerging flux regions" beneath arch filament systems which frequently recur within existing active regions. The interactions of the new and pre-existing magnetic fields frequently produce flares. The new bright structure seen only in the third images is a solar flare first seen in its early stage of development in the middle image.

The time interval between successive mosaic images in this example, 6 min 36 s, comes about as follows. The $H\alpha$ line was sampled at seven spectral positions which are the line center and alternating at three positions in the red and blue line wing. At each spectral position, 20 short exposures were made. Strictly simultaneous, there were $7 \times 20 = 140$ exposures in the nearby red continuum and other channels, in this case the G-band, blue continuum and Ca II-H. The red continuum images are used for Keller-Von der Lühe speckle reconstruction[16] of the $H\alpha$ images leading to images with diffraction limited resolution of 0.3 arcsec. This process is computer-time consuming for movies and has not yet been carried out. The frame-selected images, that are shown here, are the best of each sample of 20 images. The time required for the 140 exposures per field position is 30 s including the time needed for tuning the $H\alpha$ filter. The repositioning time of the telescope is 3 s. Hence, the cycle time per subfield is 33 s, in this case, and mosaic cycle time is $12 \times 33 = 396$ sec $= 6$ min 36 s. The additional time needed for the longer way from the last image to the first image of the next mosaic is so small that it is taken within the redundancy time built in the 3 s motion time per step. All motions are shock-free with gradual increase and decrease of the accelerations by the servo system. Longer slew distances can be obtained in short time by reaching high velocities without shocks. The same technique is used for fast tuning of the $H\alpha$ filter.

The Keller-Von der Lühe speckle reconstruction requires at least 20 images at each $H\alpha$ tuned position and about 100 images in the red continuum. This results in the following other often used tuning modes of the Hα filter including five spectral positions with each 20 images for a total of 100 images with $22 + 3 = 25$ s cycle time per subfield, 3 positions with each 34 images for a total of 102 images with $19 + 3 = 22$ s per subfield, 2 positions with each 50 images for a total of 100 images with $16 + 3 = 19$ s per subfield, and direct 100 images with $13 + 3 = 16$ s per subfield.

Surges and small flares frequently occur in and around sites where new magnetic flux is developing. It is now common knowledge that sites of new magnetic flux are marked, in $H\alpha$ images, by sets of closely spaced dark fibrils such as the set on the opposite side of the sunspot from the surge and below the filament in the right side of Figs. 5 and 6. These fibrils are much darker and are changing more rapidly than the fibrils between the sunspots in the active region in the left half of Figs. 5 and 6. The sets of dark fibrils are named "arch filament systems."[17,18] These arch filament systems, in the active region in the right side of Fig. 6, are dark because they are Doppler-shifted in varying degrees in relation to the magnetic flux emerging beneath them. They are seen as Doppler-shifted features, in Fig. 7, which shows two pair of images at wavelengths a little greater and lesser than the $H\alpha$ centerline images in Figs. 5 and 6. The first pair is at $H\alpha$ -0.04 and $+0.04$ nm from the line center wavelength of the $H\alpha$ line at 656.28 nm. On average, the Doppler shift, seen at -0.04 and $+0.04$ nm, is 18 km/s toward Earth and 18 km/s away from Earth. The second pair shows higher velocities which on average are -32 and $+32$ km/s, respectively, toward and away from Earth. Some of the arch filaments are seen to have these higher velocities which distinguish them from ordinary fibrils.

Small solar flares often occur around arch filament systems, especially around sites where one polarity of the new

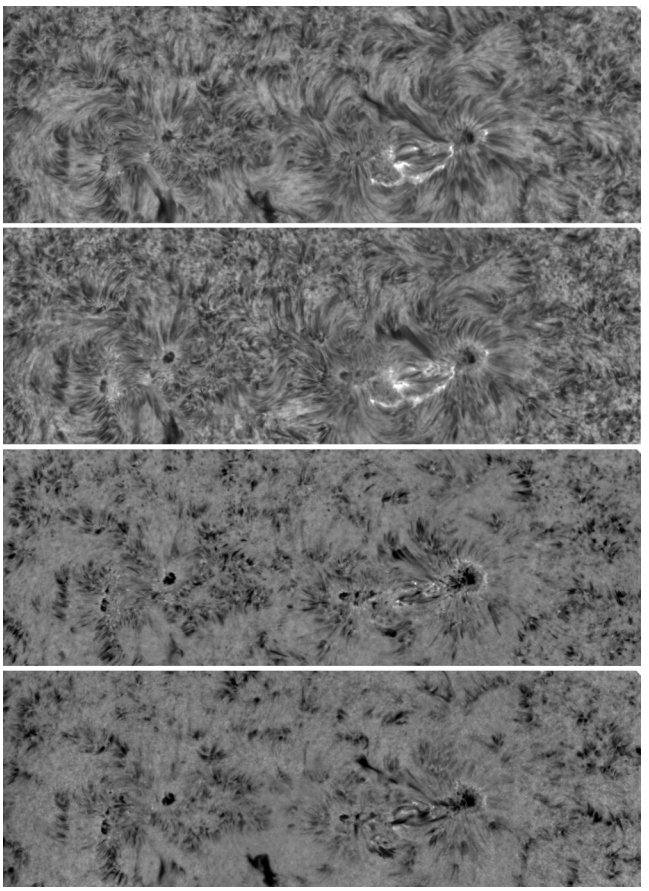

Fig. 7 The mosaic at the time of the brightening in four wing positions of the $H\alpha$ filter, from top to bottom at $+0.04$, -0.04, -0.07, and $+0.07$ nm. The flare in Fig. 6 is seen here in the near wings of $H\alpha$ in the upper pair of images below the dark arch filaments system. The flare is not seen further into the wings in the pair of images at -0.07 and $+0.07$ nm but a few arch filaments and filaments are visible due to their relatively high velocities.

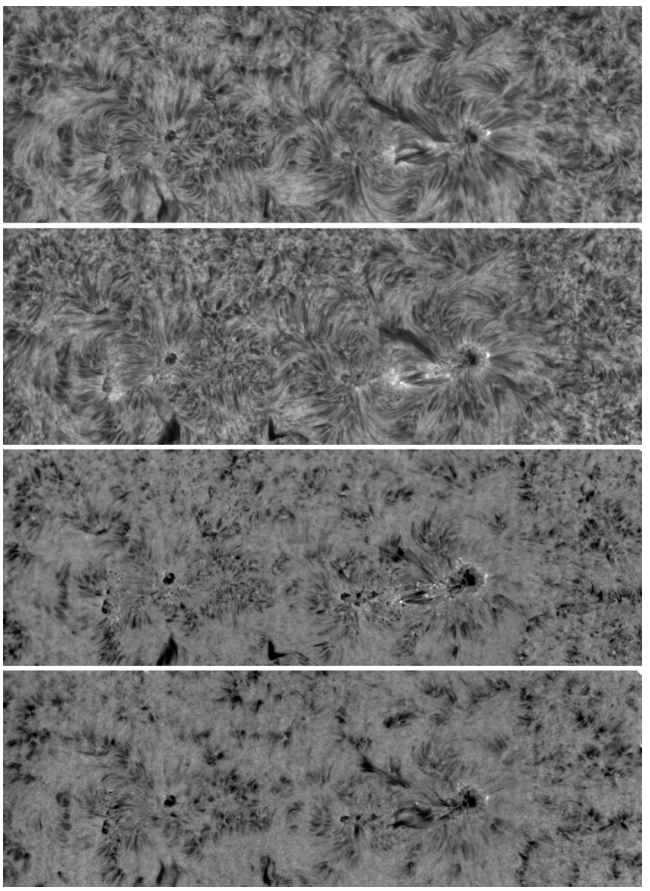

Fig. 8 The mosaic 6.6 min earlier does not show the flare seen also in the $H\alpha$ wings in Fig. 7. $H\alpha$ wings from top to bottom: $+0.04$, -0.04, -0.07, and $+0.07$ nm.

magnetic fields pushes into the surrounding magnetic field of opposite polarity. Such a flare is seen in the bottom image of Fig. 6 on and around the periphery of the arch filament system. The flare is a newly brightened area on and below the arch filament system. The flare is also seen in the top pair of images in Fig. 7. The flare is nearly identical in both images and this is evidence that the flare brightening is spectrally broadened and does not reveal Doppler shifts. Figure 8 contains the set of images that immediately preceded those in Fig. 7 for each wavelength and no flare is seen in this set. Figure 8, in comparison with Fig. 7, also reveals the Doppler shifts in the filaments quite clearly. Unlike the flare, we do not see the same filament structure in the two wings of $H\alpha$. This is typical because filaments have continuous mass motions and, therefore, their structure is slightly different in each set of images separated in time by minutes. The movies, from which the images of Figs. 6–8 are taken, can be found on the following website: http://dotdb.strw.leidenuniv.nl/ftp/DOT/2010/2010-11-13/mosaic/.

Among the direct eye-catching features are those with the greater visibility of the brightening in the blue (negative) wings, which means in the gas streams toward us. The positions, in the wings farthest away from the line center at $+$ and -0.07 nm, show the small-sized foot points of the gas streams originating low in the solar atmosphere, low-chromosphere and photosphere. The brightenings are eye catching but the longer-term development of the region is important and can be followed by the dark structures of the gas streams along the magnetic field lines. The farther away from the line center, the higher the velocities are. The wing positions, at $+$ and -0.07 nm, also show as dark structures the smaller-sized regions with higher velocities, respectively, down and upward for $+$ and $-$ wing positions. Also, some higher-up gas streams, with high velocity, are visible. The fast change of the far-wing structures is notable and typical. The time of 6.6 min between successive mosaics is too long to follow these fast changes in time in detail. Smaller mosaics would take less time. Figure 9 shows the choice on the guider disk of two smaller regions. In Fig. 9(a), a region of three by one fields and in Fig. 9(b), an image of two by two fields. It is the task of the observer to choose the best combination of field size and time resolution depending on the intended science.

Figure 10 shows an example in which the choice was to make a mosaic after a high-time-cadence single-field movie of an interesting part of the filament where many of its threads appear to connect to small-sized areas with strong magnetic fields. Figure 10(a) shows a long filament in a mosaic of a north-south strip which, in this case, is speckle reconstructed. The gap in the center part is interesting because of the many filament threads going downward into the gap and to the sides, the so-called barbs of the

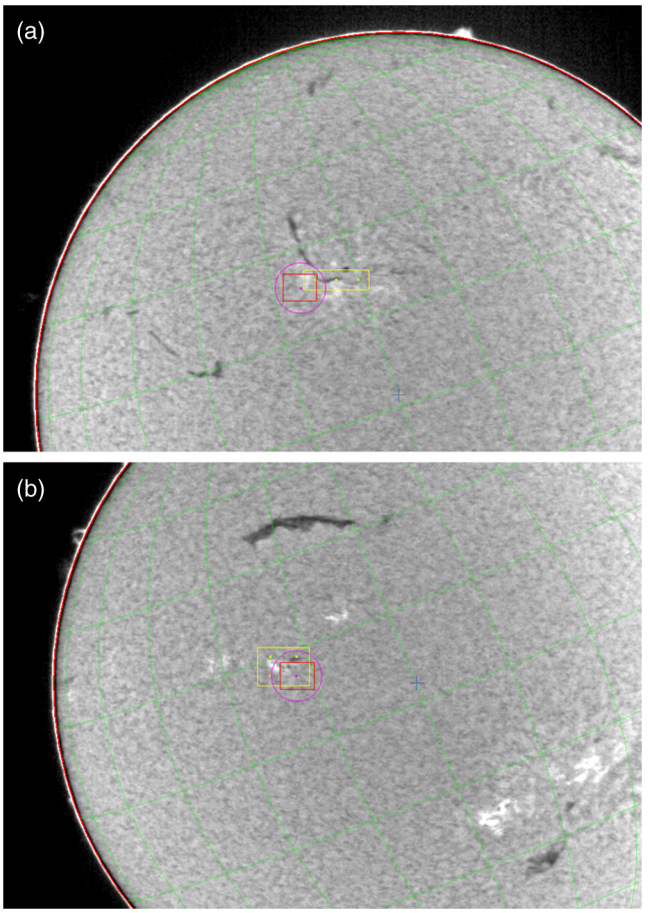

Fig. 9 Choice of two smaller mosaic regions on the guider image. (a) Region of 3×1 camera fields. (b) Region of 2×2 camera fields.

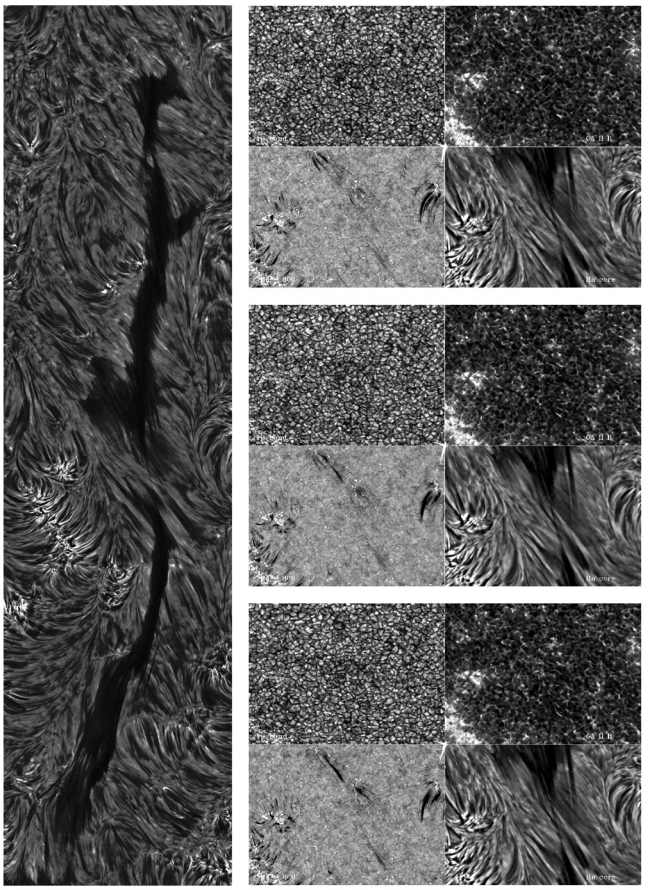

Fig. 10 (a) Mosaic of whole filament, top is north. (b) Three successive image combinations with time intervals of 30 s.

filament, where the small brightenings hint at small-scale magnetic reconnections in the lower atmosphere. The eruption of this filament was observed the next day, 7 October 2004, at Helio Research in La Crescenta, California and the eruption appeared to begin at the site of the gap. Movies, at the DOT in time cadence of 30 s, were made of a single camera field centered on this filament gap. Movies from 08:47 till 09:42 UT were speckle reconstructed. Three successive image combinations are shown in Fig. 10(b) at 09:32:00, 09:32:30 and 09:33:00 UT. Each image combination consists of a G-band image at top-left, a Ca II-H image at top-right, an $H\alpha$ core image at bottom-right, and an $H\alpha$ blue wing image at -0.08 nm of line center at bottom-left. The $H\alpha$ wing images show the very fast changes in the high-velocity gas streams in the solar atmosphere. The movie is available in avi, mov and mpeg at the DOT website: http://www.staff.science.uu.nl/~rutte101/dot/ or http://www.dot.iac.es.

Choose then "solar movies." Direct link in, for example, avi: http://www.staff.science.uu.nl/~rutte101/dot/albums/movies/2004-10-06-filament-gb+ca+haw+hac.avi.

A possibility, for very high time cadence, is to split a full burst of 100 to 140 images of the red continuum in not only spectral positions of the $H\alpha$ line but also in small time intervals. For instance, the burst of 100 images in 13 s, without tuning the $H\alpha$ filter, can be split into five successive subbursts of 20 images, each in a period of 2.6 s.

When two high-resolution telescopes are available, it is possible to combine a single camera field showing unusually

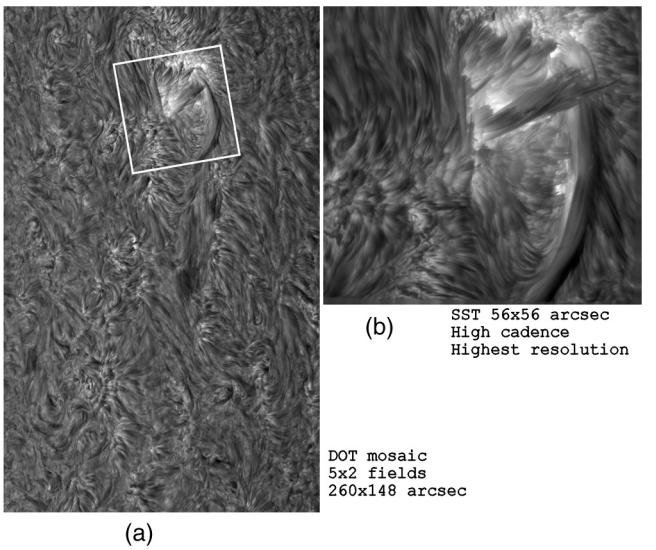

Fig. 11 (a) Mosaic including whole filament channel with interesting fast changes in high resolution but lower time cadence than for smaller field-of-view, observed by DOT. (b) Single camera field of same interesting fast changes in high resolution and high time cadence, simultaneously by SST.

fast changes in high spatial resolution and high time cadence by one of the two telescopes with simultaneous mosaics of a whole filament region around this single camera field by the other telescope. An example of such a co-observing by the SST[19] and DOT is shown in Fig. 11. These two neighboring telescopes can take advantage of good seeing at the same time for these combined observations.

5 Conclusions

The results, obtained with the observations recorded during the 2010 DOT Prominence Project of the PROM team led by Helio Research, show the capability of a new method for production of large-field mosaic movies in high spatial resolution from frame-selected images that are already suitable for movies. The time cadence of a mosaic movie is lower than that of a movie of a single camera field. The more camera fields necessary for the total mosaic field, the lower the resulting time cadence. The associated guider program offers the observer an excellent tool for choosing the best size and location of the mosaic field depending on the structures on the solar disk and the science plan.

Combinations of high-resolution mosaics, alternating with or concurrent with high-time-cadence movies of a single camera field, have proven to be valuable for revealing fast changes in specific small regions of interest within the context of evolutionary changes more suitably observed in the large mosaic fields. Sequential observations of a single field-of-view and a mosaic series of images are demonstrated, herein, using DOT observations of a single field-of-view on a gap in a filament and subsequent DOT mosaic observations of the whole filament. Collaborative observations, using two telescopes simultaneously, one to observe a single field-of-view while the other concurrently records mosaics around and including the single field-of-view, are promising. An example of such a combination demonstrates high-cadence observations of a small active region (SST) concurrent with mosaics of a large area around the active region including an adjacent long filament channel containing a filament (DOT).

Acknowledgments

We are grateful to Rob Rutten for his suggestion to start making mosaic movies and for his continuous interest in the project. The Technology Foundation STW in the Netherlands financially supported the development and construction of the DOT and follow-up technical developments. The DOT has been built by instrumentation groups of Utrecht University, the Central Workshop of Delft University (now DEMO-TU-Delft) and several firms with specialized tasks. Additional support for the DOT came from the Netherlands Organisation for Scientific Research NWO, the Netherlands Graduate School for Astronomy NOVA, and SOZOU. We acknowledge the NSF Rapid Award AGS-1024793 that made the acquisition of the data at the DOT possible during 2010. The Rapid Award was based on NSF Grant ATM-0837519 and SHINE Grant ATM 0852249 to Helio Research. We thank V. Gaizauskas to have made available to the DOT the $H\alpha$ Lyot filter. The SST and DOT are located at Observatorio del Roque de los Muchachos (ORM) of Instituto de Astrofísica de Canarias (IAC).

References

1. S. F. Martin et al., "The link between CMEs, filaments and filament channels," *Ann. Geophys.* **26**(10), 3061–3066 (2008).
2. R. Szeliski, "Video mosaics for virtual environments," *IEEE Comput. Graph. Appl.* **16**(2), 22–30 (1996).
3. A. Rav-Acha et al., "Dynamosaics: video mosaics with non-chronological time," in *Proc. IEEE Comput. Soc. Conf. on Comput. Vis. and Pattern Recognit.*, Vol. 1, pp. 58–65, IEEE, Jerusalem, Israel (2005).
4. R. J. Rutten, R. H. Hammerschlag, and F. C. M. Bettonvil, "The Dutch open telescope," in *Solar and Stellar Activity: Similarities and Differences*, C. J. Butler and J. G Doyle, Eds., Astron. Soc. Pac. Conf. Series, Vol. **158**, pp. 57–60 (1999).
5. R. J. Rutten et al., "DOT tomography of the Solar atmosphere. I. Telescope summary and program definition," *Astron. Astrophys.* **413**(3), 1183–1189 (2004).
6. DOT website: http://www.staff.science.uu.nl/~rutte101/dot/ or http://www.dot.iac.es.
7. Swedish Solar Telescope website: http://www.solarphysics.kva.se.
8. Enblend, http://enblend.sourceforge.net/.
9. Mencoder, http://www.mplayerhq.hu/.
10. G. Sliepen et al., "Contactless sub-millimeter displacement measurements," *Proc. SPIE* **7018**, 70181C (2008).
11. H. Nobach and M. Honkanen, "Two-dimensional Gaussian regression for sub-pixel displacement estimation in particle image velocimetry or particle position estimation in particle tracking velocimetry," *Exp. Fluids* **38**(4), 511–515 (2005).
12. R.H. Hammerschlag et al., "The Irkutsk Barium filter for narrow-band wide-field high-resolution solar images at the Dutch Open Telescope," *Proc. SPIE* **7735**, 773585 (2010).
13. G. I. Kushtal and V. I. Skomorovsky, "Advancements in the geometrical measurements of the birefringent filter's crystal plates and two-dimensional measurements of Doppler velocity in the solar atmosphere," *Proc. SPIE* **4900**, 504–512 (2002).
14. F. C. M. Bettonvil et al., "Tunable H-alpha Lyot filter with advanced servo system and image processing: instrument design and new scientific results with the Dutch Open Telescope," *Proc. SPIE* **6269**, 62690E (2006).
15. Helio Research website: http://www.helioresearch.org/.
16. C. U. Keller and Lühe O. von der et al., "Solar speckle polarimetry," *Astron. Astrophys.* **261**(1), 321–328 (1992).
17. A. Bruzek, "On arch-filament systems in spotgroups," *Solar Phys.* **2**(4), 451–461 (1967).
18. A. Bruzek, "Motions in arch filament systems," *Solar Phys.* **8**(1), 29–36 (1969).
19. Y. Lin et al., "Small-scale, dynamic bright blobs in solar filaments and active regions," *Astrophys. J.* **747**(2), 129 (2012).

Biographies and photographs for all authors is not available.